Inorganic Chemistry Communications 164 (2024) 112399

Contents lists available at ScienceDirect

Inorganic Chemistry Communications

journal homepage: www.elsevier.com/locate/inoche

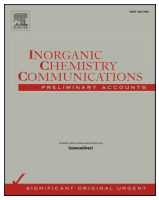

Short communication

Band gap engineering of ceria nanostructures by incorporating nitrogen-containing heterocyclic ligands

María Puerto-Jiménez [a], Daniel Goma [a,b], Almudena Aguinaco [b,c], Elena López-Maya [d], Mayra G. Álvarez [d], José María Pintado [a,b], Ginesa Blanco [a,b], Adrián Bogeat-Barroso [d,*]

[a] Departamento de Ciencia de los Materiales e Ingeniería Metalúrgica y Química Inorgánica, Facultad de Ciencias, Universidad de Cádiz, Campus Río San Pedro s/n, 11510 Puerto Real (Cádiz), Spain
[b] Instituto Universitario de Investigación en Microscopía Electrónica y Materiales (IMEYMAT), Facultad de Ciencias, Universidad de Cádiz, Campus Río San Pedro s/n, 11510 Puerto Real (Cádiz), Spain
[c] Departamento de Física de la Materia Condensada, Facultad de Ciencias, Universidad de Cádiz, Campus Río San Pedro s/n, 11510 Puerto Real (Cádiz), Spain
[d] GIR QUESCAT, Departamento de Química Inorgánica, Universidad de Salamanca, 37008 Salamanca, Spain

ARTICLE INFO

Keywords:
Ceria
1,10-Phenanthroline
Complex
Nanocubes
Optical properties

ABSTRACT

A novel facile method to prepare ceria nanocrystals with well-defined cubic morphology and enhanced optical properties is herein disclosed. Both the decrease in the band gap and the appearance of absorption edges above 400 nm, which redound in a significant absorption of visible light, are accomplished by simply incorporating *in situ* different amounts of a typical chelating bidentate ligand, 1,10-phenanthroline, during the synthesis of these ceria nanocubes. Such a remarkable effect has been tentatively connected with the ability of this nitrogen-containing heterocyclic compound to coordinate Ce^{3+} cations from the ceria precursor salt, thus yielding intermediate N 2*p* states along the band gap of the oxide.

1. Introduction

Since the mid 1970s, ceria (CeO_2) has become a ubiquitous material in the field of heterogeneous catalysis, being employed either as a catalyst or, much more frequently, as a non-inert support for catalysts and as a structural or electronic promoter [1,2]. Indeed, ceria is an essential material in the manufacture of modern three-way catalysts (TWCs), which is the most widespread and important catalytic application of this rare earth oxide in terms of establishment, economic relevance, and tonnage [2].

The coordination chemistry of both cerium(III) and cerium(IV) cations has been profusely investigated over the last few decades, as evidenced by the large number of complexes formed with a variety of ligands whose preparation and characterisation have been reported in the literature ([3–9] and references therein). The development of this research field has been pushed forward by the widespread applications of cerium complexes in organic synthesis, catalysis, magnetism, luminescence, and biomedical sciences [8,10]. Nevertheless, to the best of our knowledge, the incorporation of functional-organic compounds into the ceria structure through their coordination to cerium cations remains unexplored. Such coordination is expected to remarkably alter both the crystal and electronic structure of this rare earth oxide, which likely redounds in promising modifications of its physicochemical features, including optical, electrical, and magnetic properties. If precisely controlled, these changes could pave the way for improving the performance and expanding the applications of ceria, particularly in the field of heterogeneous catalysis and photocatalysis. Indeed, a similar approach has been recently implemented by García-Martínez's group to successfully enhance both the optical properties and photocatalytic activity of titania (TiO_2). In a set of works, they incorporated *in situ* several organic compounds, such as chromogenic molecules (4,6-dihydroxypyrimidine [11] and *p*-phenylenediamine [11,12]), amino acids (L-tyrosine [13]), and chelating heterocyclic ligands (1,10-phenanthroline [14]), into the titania lattice during its synthesis by a conventional sol–gel method from alkoxide precursors, under mild conditions and at low temperatures. The resulting materials, referred to as "organo-titanias", exhibited a reduced band gap together with a high photocatalytic efficiency towards the degradation of model organic pollutants (rhodamine 6G, rhodamine B, and methylene blue) in aqueous solution under visible light irradiation.

Herein, we investigate for the first time the effect of incorporating *in situ* a classic, nitrogen-containing, heterocyclic organic ligand, namely

* Corresponding author.
E-mail address: adrianbogeat@usal.es (A. Bogeat-Barroso).

https://doi.org/10.1016/j.inoche.2024.112399
Received 2 January 2024; Received in revised form 29 March 2024; Accepted 5 April 2024
Available online 5 April 2024

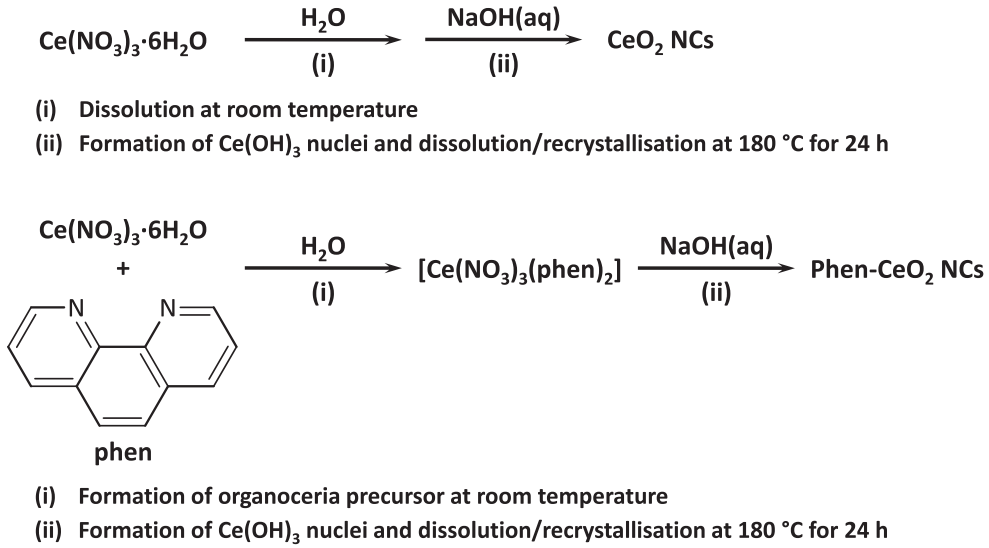

Fig. 1. Schematic illustration of the synthesis of the reference phen-free ceria nanocubes (up) and the ceria-phen nanostructured hybrid materials (down), using the same experimental conditions.

1,10-phenanthroline (phen, henceforth), during the preparation of crystallographically well-defined ceria nanoparticles with cubic morphology by a conventional, surfactant-free, hydrothermal method operating under mild conditions. In addition to a versatile chelating character [15], which allows this molecule to form complexes with a variety of transition metal and lanthanoid cations, including cerium(III) [16–19], phen has been selected as ligand because of its excellent electron transport and hole blocking properties [20], both being highly desirable with a view to developing more efficient photocatalysts. The resulting "organoceria" nanostructured hybrid materials benefit from the combination of the unique catalytic properties of ceria nanocubes, which mostly expose {1 0 0} facets with improved reducibility [21,22], and the boost in the optical properties brought by the incorporation of phen in their fluorite-type crystal structure.

In summary, the present work discloses a unique wet-chemistry synthetic strategy to prepare nanostructured ceria particles under mild conditions, featuring well-defined controlled morphology and incorporating an organic compound as modifier via its coordination to lattice cerium atoms. Furthermore, this novel approach also allows to exert a tunable control over the band gap of the resulting organocerias due to the presence of cerium-nitrogen bonds, which act as a source of intermediate N 2*p* states.

2. Materials and methods

A set of ceria-phen nanostructured hybrid materials featuring well-defined cubic morphology was prepared by modifying the facile hydrothermal method earlier described by H.-X. Mai [21]. As schematically summarised in Fig. 1, a complex between the ceria precursor (*i.e.*, $Ce(NO_3)_3{\cdot}6H_2O$) and the phen ligand was firstly synthesised by direct reaction in deionised water at room temperature. After vigorous mechanical stirring for at least 2 h, the initial colourless clear solutions turned into pale yellowish solutions/suspensions. Such visual change is connected with the formation of a neutral cerium complex with the chemical formula $[Ce(NO_3)_3(phen)_2]$. According to the literature [17], its structure has been reported to consist of a ten-fold coordinated Ce^{3+} cation, which is surrounded by four nitrogen atoms from the couple of phen molecules and six oxygen atoms belonging to the three nitrate ions. Therefore, the coordination polyhedron around the rare earth atom is described as a distorted bicapped square antiprism. In parallel with the synthesis of the organoceria samples, the isolation of bright yellow single crystals of this complex was successfully accomplished by slow evaporation of the aqueous solvent at room temperature for several days. The resulting crystalline solid has been taken as a reference material with a view to clarifying the incorporation of the phen ligand into the lattice of the organoceria samples and its coordination to the cerium atoms by means of spectroscopic techniques, as will be discussed later. In a second step, the aqueous suspensions of the aforesaid cerium complex were employed as precursors for the hydrothermal synthesis of the ceria-phen nanostructured hybrid materials, under a NaOH concentration of 9 mol·L^{-1} at 180 °C for 24 h. Three different Ce/phen molar ratios, namely 8, 12, and 24, were tested, so that the resulting organocerias are henceforth referred to as XPhen-CeO_2 NCs, where the figure X denotes the nominal Ce/phen molar ratio. Further details on the experimental synthetic procedure are provided in the SI file.

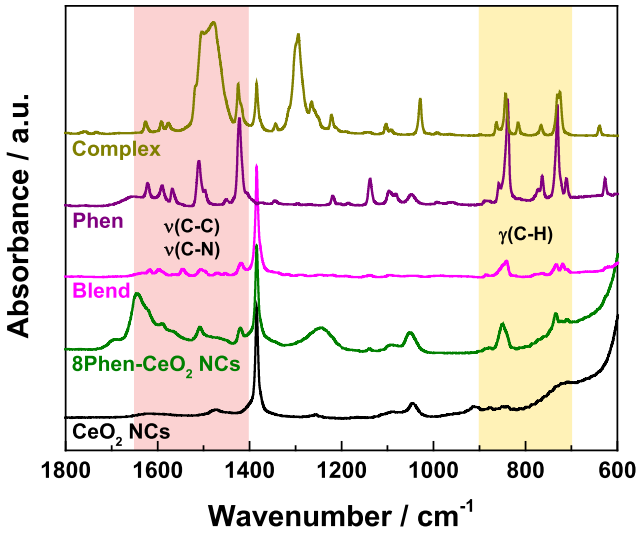

Fig. 2. FT-IR spectrum of the 8Phen-CeO_2 NCs hybrid material, together with those registered for the reference phen-free ceria nanocubes sample, pure phen, and their physical blend in a 8:1 molar ratio (*ca.* 11.6 wt% phen) for comparison purposes.

3. Results and discussion

Phen incorporation into the lattice of the nanostructured hybrid

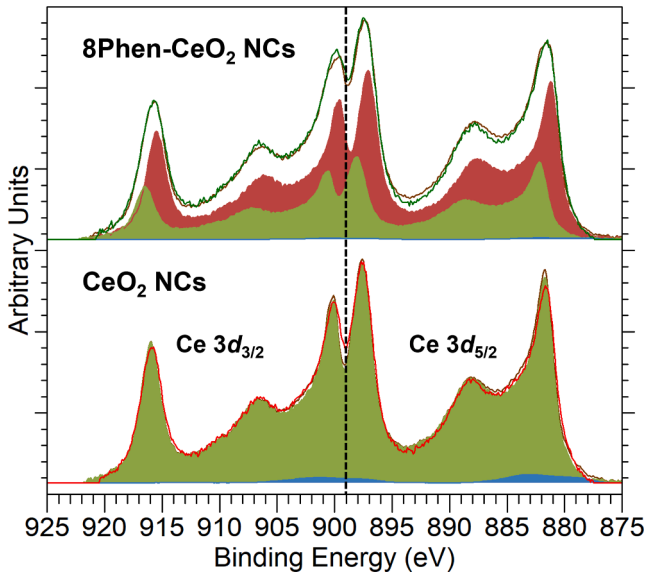

Fig. 3. XPS spectra corresponding to Ce 3*d* core level of 8Phen-CeO_2 NCs and the reference phen-free CeO_2 NCs.

materials was firstly investigated by Fourier transform infrared (FT-IR) spectroscopy. Fig. 2 gathers the spectrum of the 8Phen-CeO_2 NCs sample, together with those registered for the reference materials CeO_2 NCs and pure phen, their physical blend in a 8:1 molar ratio (*i.e.*, *ca.* 11.6 wt % phen), and the $[Ce(NO_3)_3(phen)_2]$ complex. Particular attention should be paid to those frequency regions in which the most distinctive vibrations of the heterocyclic ligand appear, namely from 1650 to 1400 cm^{-1} for the stretching vibration modes (ν) of C-C and C-N aromatic bonds, and between 900 and 700 cm^{-1} for out-of-plane bending vibrations (γ) of C-H bonds [23,24]. Accordingly, the appearance of the four most intense absorption peaks of phen, ascribable to ν(C-C), ν(C-N), and γ(C-H) vibrations of the hydrogen atoms on both the heterocyclic rings and the centre ring, in the infrared spectrum of 8Phen-CeO_2 NCs unambiguously confirms the presence of the ligand in this nanomaterial. A close examination of such spectrum clearly reveals that the ν(C-C) and ν(C-N) peaks undergo a shift towards slightly lower frequencies as compared to their original positions for pristine phen, while just the opposite trend is noticed for those spectral features attributable to the γ(C-H) vibrations. This finding is indicative of the coordination of phen to cerium atoms of the ceria lattice, well in agreement with the displacements observed for the aforesaid main signals in the infrared spectrum acquired for the $[Ce(NO_3)_3(phen)_2]$ complex, and also with the results previously reported elsewhere for a variety of metal-phen complexes [23,25,26]. Furthermore, the intensity of these distinctive peaks increases with the nominal phen content in the organoceria samples, whereas their frequencies remain unaltered (see Fig. S1). On

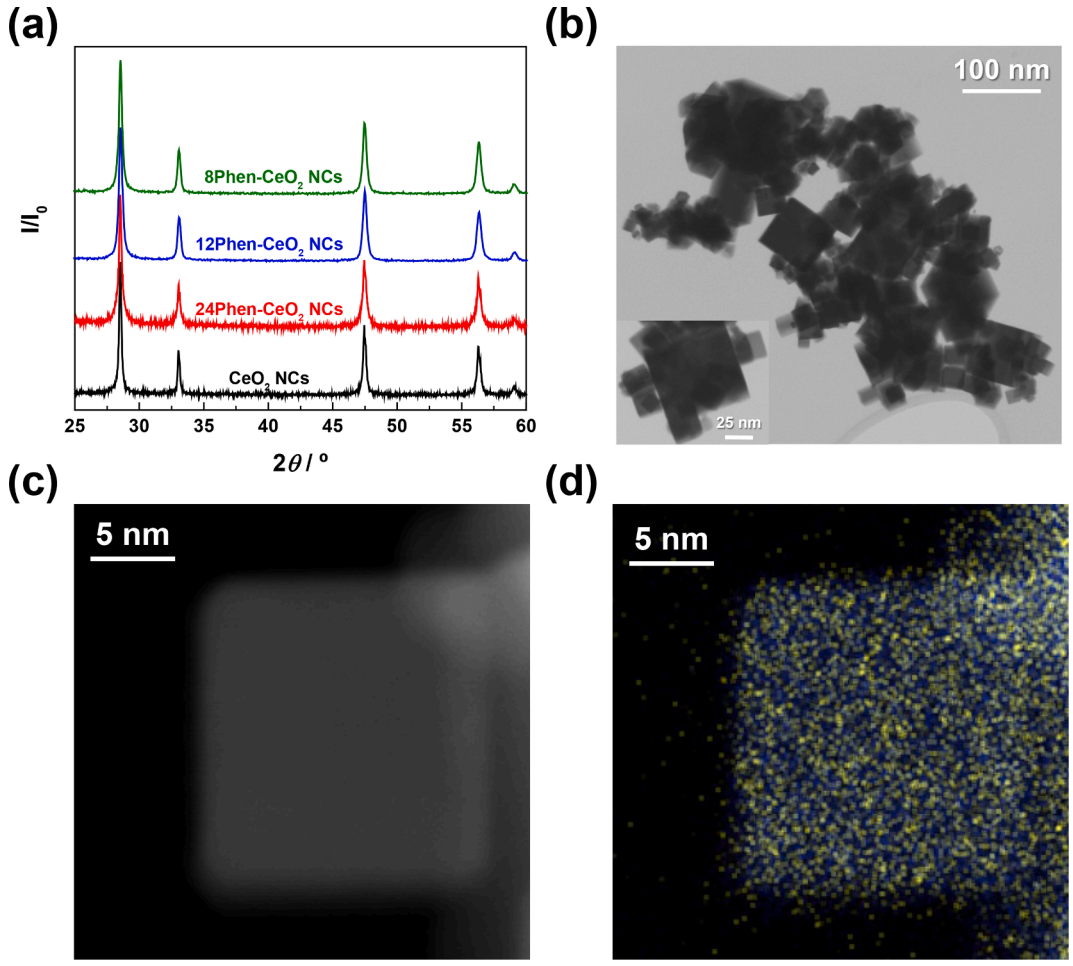

Fig. 4. (a) PXRD diagrams recorded for the ceria-phen nanostructured hybrid materials and the reference phen-free ceria nanocubes sample, (b) representative STEM images for 8Phen-CeO_2 NCs, (c) HAADF-STEM image for a single nanocube of the 8Phen-CeO_2 NCs sample, and (d) its corresponding X-EDS map displaying the distribution of cerium (blue) and nitrogen (yellow). (For interpretation of the references to colour in this figure legend, the reader is referred to the web version of this article.)

the other hand, it is also worth mentioning that, as expected, no changes in both the position and relative intensity of the main infrared spectral features of phen are detected after its physical blend with the control CeO_2 NCs sample.

The above conclusion on the effective phen incorporation into the ceria lattice through its coordination to cerium atoms was further confirmed from X-ray photoelectron spectroscopy (XPS) analyses. The survey spectra also reveal the presence of both carbon and nitrogen in all three organoceria samples, in addition to the elements cerium and oxygen. Regarding the high-resolution spectra and derived quantitative data, several major issues are worth discussing. The first one refers to the oxidation state of the lanthanoid element. In stark contrast to the phen-free ceria reference nanomaterial, whose Ce^{3+} fraction in the outermost surface layers amounts to around 3 %, the detailed analysis of the Ce 3*d* core level signals (see Fig. 3 and S2(a)) for the phen-doped samples indicates that the oxidation state of surface cerium was exclusively + 4. Accordingly, phen incorporation into the ceria lattice appears to bring about a dramatic drop in the Ce^{3+} concentration at surface level, up to a depth of around 3.5 nm. A second point of interest relates to the chemical environment of the Ce^{4+} cations in the organocerias. Ce 3*d* core level spectrum is rather complex, consisting of a multiplet structure made up of a set of three peaks for each $3d_{5/2}$ and $3d_{3/2}$ components, provided that both Ce^{4+} and Ce^{3+} are present in the material [27]. In order to avoid possible errors in the fitting procedure of the spectra by employing such a large set of peaks, two high resolution spectra, corresponding to samples with either 100 % Ce^{3+} or 100 % Ce^{4+} contents, were used as references. Unlike the Ce 3*d* spectrum for the CeO_2 NCs sample, those collected for the phen-containing nanomaterials could not be properly fitted by means of the aforesaid complex peaks structure. Instead, they display as most striking feature unusually broad peaks, which can be only interpreted on the basis of the coexistence in these hybrid materials of Ce^{4+} cations with two fairly different chemical environments. Thus, an important fraction of these ions, whose main peak is centred in the range 897.5–898 eV, are in a typical fluorite oxide environment, while some other Ce^{4+} are coordinated by the phen molecule, with their most intense peak appearing at somewhat lower binding energies (BE). In this connection, it should be noted that the unusual width was only detected for the Ce 3*d* core level signals, thus allowing to rule out an effect related to a poor charge compensation. The third issue worth commenting on concerns the N 1*s* region, which shows a clearly visible peak at around 398.8 eV (see Fig. S2(b)). This signal is slightly shifted to lower BE as compared to its position for pure phen [28], thus proving the effective complexation of its nitrogen atoms with cerium. Accordingly, it is concluded that the Ce-N coordination bonds initially established in aqueous solution during the first synthetic step remain to some extent in the resulting organoceria samples, in spite of the fact that the oxidation state of cerium changed from +3 to +4 during the preparation process. Finally, as expected the intensity of the N 1*s* peak increases with the ligand content in the phen-doped nanomaterials.

Once the effectiveness in the phen incorporation into the ceria structure was evidenced by means of spectroscopic techniques, the actual content of this organic compound in each of the hybrid nanomaterials was assessed from thermogravimetric (TG) analyses in flowing oxygen. The resulting TG-DTG curves shown in Fig. S3 display a remarkable mass loss spanning from 300 °C up to 400 °C, with the maximum rate at around 360 °C. As expected, such thermal effect is attributed to the complete combustion of phen. Furthermore, the thermal decomposition of this molecule is noticeably delayed (*ca.* 100 °C) in comparison with the pure compound [14], thus supporting the conclusions previously drawn on its incorporation into the ceria structure and coordination to cerium atoms. The total phen contents in the organoceria solids, as estimated from their TG plots, are markedly lower than the corresponding nominal values, with incorporation yields of around 20 % regardless of the starting Ce/phen molar ratio (see Tables 1 and S1). Therefore, it becomes evident that an important fraction of the organic compound either remained in solution or was decomposed under the synthesis conditions employed during the hydrothermal treatment. However, despite the relatively low phen contents of the hybrid nanomaterials, their effect on the band gap of pure ceria was dramatic, as will be discussed later.

Table 1
Phen content, textural and structural parameters, and band gap energy values for the ceria-phen nanostructured hybrid materials and the reference phen-free ceria nanocubes.

Sample	Phen[a]/wt %	S_{BET}[b]/ $m^2 \cdot g^{-1}$	D[c]/ nm	D[d]/ nm	$d_{(1\,1\,1)}$[e]/ Å	E_g[f]/ eV
CeO_2 NCs	–	20.5	46.5	47.0	3.124	3.23
24Phen-CeO_2 NCs	0.90	27.8	38.7	40.3	3.125	3.17
12Phen-CeO_2 NCs	1.84	29.5	25.5	27.3	3.126	3.11
8Phen-CeO_2 NCs	2.23	20.9	30.5	28.9	3.125	3.06

[a] Actual phen content from TG analyses.
[b] BET specific surface area from N_2 adsorption/desorption isotherms at −196 °C.
[c] Average crystallite size as estimated from PXRD.
[d] Mean particle size as determined from STEM.
[e] Ceria lattice spacing from PXRD.
[f] Band gap energy as calculated from the intercept of the tangent to the $(F(R')h\nu)^{1/2}$ *vs.* the $(h\nu)$ plot.

After verifying the effective incorporation of the phen molecule into the ceria, the crystalline structure of the as-synthesised organocerias was investigated by powder X-ray diffraction (PXRD). The recorded diffractograms for these hybrid materials and the reference phen-free ceria nanocubes sample are depicted in Fig. 4(a). As can be seen, they are all dominated by a set of well-defined reflections ascribable to CeO_2 with cubic fluorite-type structure (space group *Fm*-3*m*, JCPDS 34–0394). Furthermore, no diffraction peaks associated with other cerium-containing crystalline phases are detected in the diagrams after phen incorporation, thus allowing to exclude a biphasic structure. The only distinctive feature of these patterns is a slight broadening of their peaks (see Fig. S4), which points to a reduction in the average crystallite size for the organoceria hybrid nanomaterials. In fact, this latter parameter, as assessed by applying the Scherrer equation to the main diffraction peak of ceria at 28.5°, decreases from around 45 nm for the organic-free control ceria sample up to 25–38 nm for its phen-containing counterparts (see Table 1). This finding advocates for a certain hindrance to the crystallisation of the ceria phase during the hydrothermal treatment, because of the phen incorporation into the oxide structure through its coordination to cerium atoms. Finally, the lattice spacing estimated for the organocerias from their PXRD patterns is quite consistent with the distance between (1 1 1) crystal planes of the ceria phase (*i.e.*, 3.12 Å). Nonetheless, from Table 1 a very modest increase in this interplanar distance is also noted as a result of the strain associated with the introduction of the relatively large heterocyclic molecule (as a reference, a mean size of *ca.* 0.70 nm has been estimated for phenanthrene [29], a polycyclic aromatic compound with a molecular structure closely related to that of phen). Such a strain effect due to the incorporation of phen could be also responsible, to some extent, for the abovementioned broadening of the reflection peaks.

As far as the morphological features of the ceria-based nanomaterials are concerned, the representative scanning-transmission electron microscopy (STEM) images gathered in Fig. 4(b) clearly evidence that they are indeed made up of well-defined cubic-shaped nanocrystals, which are chiefly enclosed by {1 0 0} surfaces. Moreover, their edge lengths are in the range from 5 to 80 nm, the average values being somewhat smaller for the phen-containing samples as previously suggested by the mean crystallite sizes derived from PXRD. In this connection, such a reduction in the crystallite size brings about a significant increase in the specific surface area (S_{BET}) from 20.5 $m^2 \cdot g^{-1}$ for the control organic-free sample to nearly 30 $m^2 \cdot g^{-1}$ for the phen-doped nanomaterials. By

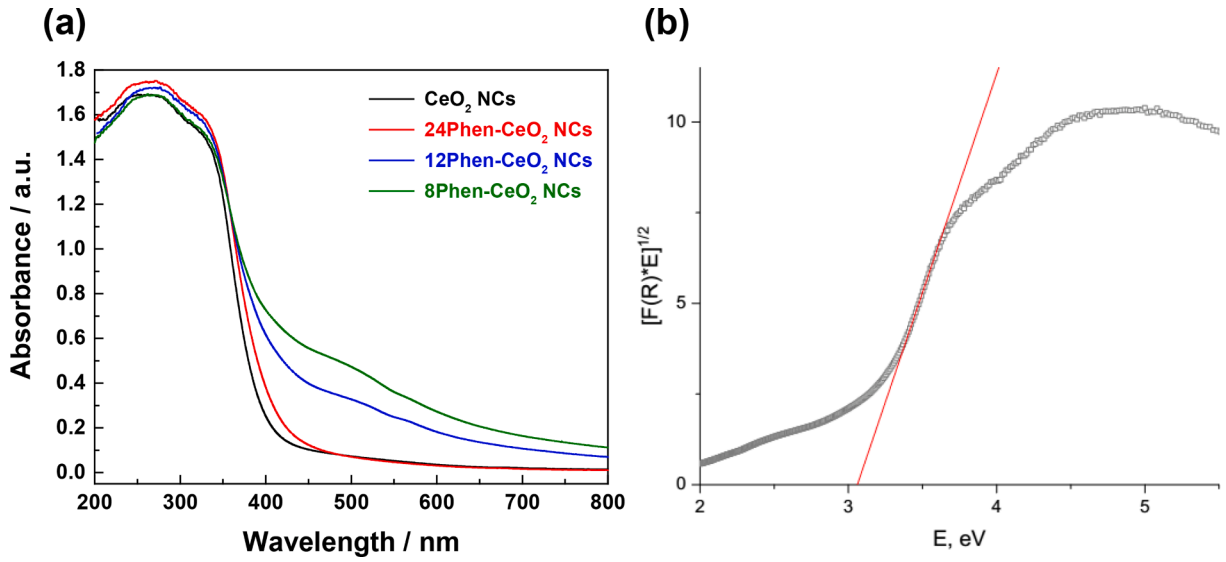

Fig. 5. (a) DRUV spectra registered for the ceria-phen nanostructured hybrid materials and the reference phen-free ceria nanocubes sample and (b) Tauc plot of the transformed Kubelka-Munk function *vs.* the energy of light absorbed for 8Phen-CeO_2 NCs.

bearing in mind these results, it may be concluded that the incorporation of phen during the synthesis of the ceria nanocubes does not entail any change in the morphology, but only affects the crystallite size by hindering the crystallisation of the ceria phase.

In order to confirm the actual spatial distribution of nitrogen, which is closely connected with that of the phen molecule, X-EDS analyses were performed on both the undoped and phen-doped ceria nanomaterials. The chemical map acquired for a single nanocube representative of the 8Phen-CeO_2 NCs sample is shown in Fig. 4(d), with signals corresponding to cerium and nitrogen depicted in blue and yellow, respectively. The map clearly illustrates the homogeneous distribution of this latter element throughout the mass of the nanoparticle, spanning its entire volume. Accordingly, it may be concluded that the phen ligand is evenly incorporated into the ceria nanocubes during the hydrothermal synthesis process.

Finally, the potential suitability of the as-prepared ceria-phen nanostructured hybrid materials for photocatalytic applications strongly relies on their activation under visible light irradiation. Among other strategies, this challenge could be overcome by reducing their band gap, *i.e.*, by changing the relative positions of both the conduction and valence bands through the selective introduction of intermediate energetic states. As inferred from Table 1 and Fig. 5(b), the incorporation of phen during the synthesis of the ceria nanocubes leads to a remarkable decrease in the band gap value from 3.23 eV for the organic-free control material down to 3.06 eV for the 8Phen-CeO_2 NCs sample. Such an effect is likely ascribed to the presence of intermediate N 2*p* energy levels coming from the Ce-N coordination bonds, which are preserved throughout the whole preparation process of the hybrid nanomaterials. These intermediate levels would be responsible for the activation of the organocerias under visible light irradiation. Moreover, the additional absorption edges appearing above 400 nm in the diffuse reflectance ultraviolet (DRUV) spectra for the ceria-phen hybrid nanomaterials (see Fig. 5(a)) are also consistent with the appearance of the aforesaid intraband gap states [30]. Therefore, long wavelength visible light irradiation is able to generate electron-hole pairs in these organoceria samples.

4. Conclusions

In conclusion, we have developed a novel strategy to prepare ceria nanocrystals featuring a well-defined cubic morphology and improved optical properties. Our synthetic approach relies on incorporating small amounts of phen during the preparation of the ceria nanocubes by a conventional hydrothermal method under mild conditions. By coordinating with the cerium atoms of the ceria lattice, this nitrogen-containing heterocyclic ligand is able to introduce intermediate N 2*p* energy levels along the band gap of the oxide, thus allowing the activation of the resulting organocerias under visible light irradiation. Thus, the proposed methodology represents a facile, wet-chemistry, alternative to conventional strategies for band gap reduction of ceria, such as nitrogen doping and creation of oxygen vacancies by thermal treatment.

CRediT authorship contribution statement

María Puerto-Jiménez: Investigation. **Daniel Goma:** Visualization, Validation, Resources, Investigation, Formal analysis. **Almudena Aguinaco:** Visualization, Investigation, Formal analysis. **Elena López-Maya:** Writing – review & editing. **Mayra G. Álvarez:** Writing – review & editing, Investigation, Funding acquisition. **José María Pintado:** Writing – review & editing, Resources, Methodology. **Ginesa Blanco:** Writing – review & editing, Visualization, Supervision, Methodology, Investigation, Funding acquisition, Formal analysis, Conceptualization. **Adrián Bogeat-Barroso:** Writing – review & editing, Writing – original draft, Visualization, Validation, Supervision, Methodology, Investigation, Formal analysis, Conceptualization.

Declaration of competing interest

The authors declare that they have no known competing financial interests or personal relationships that could have appeared to influence the work reported in this paper.

Data availability

Data will be made available on request.

Acknowledgements

Financial support from the Spanish Ministry of Science and Innovation and FEDER Program of EU (project PID2020-113006RB-I00) and from the University of Salamanca (Research Program I, C2 call, project PIC2-2022-08) is gratefully acknowledged. Electron microscopy studies were accomplished by using the equipment available at the DME-UCA node of the Spanish Unique Infrastructure (ICTS) on Electron

Microscopy of Materials (ELECMI).

Appendix A. Supplementary data

Supplementary data to this article can be found online at https://doi.org/10.1016/j.inoche.2024.112399.

References

[1] A. Trovarelli, P. Fornasiero, Catalysis by ceria and related materials, 2nd editio, Imperial College Press, London, 2013.

[2] T. Montini, M. Melchionna, M. Monai, P. Fornasiero, Fundamentals and catalytic applications of CeO2-based materials, Chem. Rev. 116 (2016) 5987–6041, https://doi.org/10.1021/acs.chemrev.5b00603.

[3] T. Moeller, D.F. Martin, L.C. Thompson, R. Ferrús, G.R. Feistel, W.J. Randall, The coordination chemistry of yttrium and the rare earth metal ions, Chem. Rev. 65 (1965) 1–50, https://doi.org/10.1021/cr60233a001.

[4] F.T. Edelmann, Lanthanide amidinates and guanidinates: from laboratory curiosities to efficient homogeneous catalysts and precursors for rare-earth oxide thin films, Chem. Soc. Rev. 38 (2009) 2253–2268, https://doi.org/10.1039/b800100f.

[5] S.A. Cotton, J.M. Harrowfield, Lanthanides: coordination chemistry, Encycl. Inorg. Bioinorg. Chem. (2012), https://doi.org/10.1002/9781119951438.eibc2062.

[6] F.M.A. Sroor, F.T. Edelmann, Lanthanides: tetravalent organometallic, Encycl. Inorg. Bioinorg. Chem. (2012), https://doi.org/10.1002/9781119951438.eibc2034.

[7] V.E. Pushkarev, L.G. Tomilova, V.N. Nemykin, Historic overview and new developments in synthetic methods for preparation of the rare-earth tetrapyrrolic complexes, Coord. Chem. Rev. 319 (2016) 110–179, https://doi.org/10.1016/j.ccr.2016.04.005.

[8] Y.-M. So, W.-H. Leung, Recent advances in the coordination chemistry of cerium (IV) complexes, Coord. Chem. Rev. 340 (2017) 172–197, https://doi.org/10.1016/j.ccr.2016.12.009.

[9] H. Tsurugi, K. Mashima, Renaissance of homogeneous cerium catalysts with unique Ce(IV/III) couple: redox-mediated organic transformations involving homolysis of Ce(IV)-ligand covalent bonds, J. Am. Chem. Soc. 143 (2021) 7879–7890, https://doi.org/10.1021/jacs.1c02889.

[10] M. Patyal, K. Kaur, N. Bala, N. Gupta, A.K. Malik, Innovative lanthanide complexes: Shaping the future of cancer/tumor chemotherapy, J. Trace Elem. Med. Biol. 80 (2023) 127277, https://doi.org/10.1016/j.jtemb.2023.127277.

[11] M. Rico-Santacruz, Á.E. Sepúlveda, E. Serrano, E. Lalinde, J.R. Berenguer, J. García-Martínez, Organotitanias: a versatile approach for band gap reduction in titania based materials, J. Mater. Chem. C. 2 (2014) 9497–9504, https://doi.org/10.1039/c4tc01704h.

[12] J. Jiménez-López, N. Linares, E. Serrano, J. García-Martínez, Visible-Light-activated black organotitanias: how synthetic conditions influence their structure and photocatalytic activity, Chempluschem. 83 (2018) 390–400, https://doi.org/10.1002/cplu.201800054.

[13] G. Sarigul, I. Chamorro-Mena, N. Linares, J. García-Martínez, E. Serrano, Hybrid amino acid-TiO2 materials with tuneable crystalline structure and morphology for photocatalytic applications, Adv. Sustain. Syst. 5 (2021) 2100076, https://doi.org/10.1002/adsu.202100076.

[14] G. Sarigul, I. Gómez-Palos, N. Linares, J. García-Martínez, R.D. Costa, E. Serrano, The use of N^N ligands as an alternative strategy for the sol-gel synthesis of visible-light activated titanias, J. Mater. Chem. C. 8 (2020) 12495–12508, https://doi.org/10.1039/d0tc03073b.

[15] A. Bencini, V. Lippolis, 1,10-Phenanthroline: A versatile building block for the construction of ligands for various purposes, Coord. Chem. Rev. 254 (2010) 2096–2180, https://doi.org/10.1016/j.ccr.2010.04.008.

[16] F.A. Hart, F.P. Laming, Complexes of 1,10-phenanthroline with lanthanide chlorides and thiocyanates, J. Inorg. Nucl. Chem. 26 (1964) 579–585, https://doi.org/10.1016/0022-1902(64)80291-8.

[17] Q.-Y. Lin, Y.-L. Feng, Crystal structure of tris(nitrato-O, O')bis(1,10-phenanthroline-N, N')-cerium (III), Ce (NO3)3(C12H8N2)2, Zeitschrift Für Krist - New Cryst. Struct. 218 (2003) 531–532, https://doi.org/10.1524/ncrs.2003.218.4.531.

[18] B.P. Nibha, G. Baranwal, C.G. Singh, Daniliuc, Synthesis, characterization and thermolysis of lanthanide metal nitrate complexes with 1,10-phenanthroline, Part-95, J. Rare Earths. 32 (2014) 545–552, https://doi.org/10.1016/S1002-0721(14)60106-X.

[19] A.V. Shurygin, V.I. Vovna, V.V. Korochentsev, A.G. Mirochnik, I.V. Kalinovskaya, V.I. Sergienko, Electronic structure and optical properties of Ln(III) nitrate adducts with 1,10-phenanthroline, Spectrochim. Acta - Part A Mol. Biomol Spectrosc. 213 (2019) 176–183, https://doi.org/10.1016/j.saa.2019.01.033.

[20] C. Sun, Y. Wu, W. Zhang, N. Jiang, T. Jiu, J. Fang, Improving efficiency by hybrid TiO2 nanorods with 1,10-phenanthroline as a cathode buffer layer for inverted organic solar cells, ACS Appl. Mater. Interfaces. 6 (2014) 739–744, https://doi.org/10.1021/am404423k.

[21] H.-X. Mai, L.-D. Sun, Y.-W. Zhang, R. Si, W. Feng, H.-P. Zhang, H.-C. Liu, C.-H. Yan, Shape-selective synthesis and oxygen storage behavior of ceria nanopolyhedra, nanorods, and nanocubes, J. Phys. Chem. B. 109 (2005) 24380–24385, https://doi.org/10.1021/jp055584b.

[22] T. Désaunay, G. Bonura, V. Chiodo, S. Freni, J.-P. Couzinié, J. Bourgon, A. Ringuedé, F. Labat, C. Adamo, M. Cassir, Surface-dependent oxidation of H2 on CeO2 surfaces, J. Catal. 297 (2013) 193–201, https://doi.org/10.1016/j.jcat.2012.10.011.

[23] A.A. Schilt, R.C. Taylor, Infra-red spectra of 1:10-phenanthroline metal complexes in the rock salt region below 2000 cm-1, J. Inorg. Nucl. Chem. 9 (1959) 211–221, https://doi.org/10.1016/0022-1902(59)80224-4.

[24] S.S. Singh, Infrared spectra of 1:10 phenanthroline and its addition compounds with antimony trichloride and antimony pentachloride, Zeitschrift Fur Naturforsch. - Sect A J. Phys. Sci. 24 (1969) 2015–2016, https://doi.org/10.1515/zna-1969-1227.

[25] M.M. Campos-Vallette, R.E. Clavijo, F. Mendizabal, W. Zamudio, R. Baraona, G. Diaz, Infrared spectrum of the bis-(1,10-phenanthroline) Cu(I) and Cu(II) perchlorate complexes, Vib. Spectrosc. 12 (1996) 37–44, https://doi.org/10.1016/0924-2031(96)00012-4.

[26] D.J. Awad, F. Conrad, A. Koch, U. Schilde, A. Pöppl, P. Strauch, 1,10-Phenanthroline-dithiolate mixed ligand transition metal complexes. Synthesis, characterization and EPR spectroscopy, Inorg. Chim. Acta. 363 (2010) 1488–1494, https://doi.org/10.1016/j.ica.2010.01.021.

[27] A. Kotani, H. Ogasawara, Interplay between intra-atomic multiplet coupling and interatomic hybridization in core-level spectroscopy, J. Electron Spectros. Relat. Phenomena. 86 (1997) 65–72, https://doi.org/10.1016/s0368-2048(97)00050-9.

[28] C. Ferragina, M.A. Massucci, G. Mattogno, XPS studies on the host-guest interaction of 2,2′-bipyridyl, 1,10-phenanthroline and 2,9-dimethyl-1,10-phenanthroline intercalated in α-zirconium phosphate, J. Incl. Phenom. Mol. Recognit. Chem. 7 (1989) 529–536, https://doi.org/10.1007/BF01080463.

[29] A.M. Mastral, T. García, M.S. Callén, M.V. Navarro, J. Galbán, Removal of naphthalene, phenanthrene, and pyrene by sorbents from hot gas, Environ. Sci. Technol. 35 (2001) 2395–2400, https://doi.org/10.1021/es000152u.

[30] P. Makuła, M. Pacia, W. Macyk, How to correctly determine the band gap energy of modified semiconductor photocatalysts based on UV-Vis spectra, J. Phys. Chem. Lett. 9 (2018) 6814–6817, https://doi.org/10.1021/acs.jpclett.8b02892.